Available online at https://sej.journals.ekb.eg/

FACULTY OF ENGINEERING – SOHAG UNIVERSITY

Sohag Engineering Journal (SEJ), VOL. 2, NO. 2, SEPTEMBER 2022

CYCLICALLY LOADED GFRP RC MID-RISE WALLS: PARAMETRIC RESEARCH

Nourhan Ahmed[a], Ahmed Attia[a*], Mamdouh Abbas Kenawy[a], Mohamed F. M. Fahmy[b]

[a]*Civil Engineering Department, Faculty of Engineering, Sohag University, Sohag, 82524, Egypt*
[b]*Civil Engineering Department, Faculty of Engineering, Assiut University, 71515, Egypt*

Abstract

In this paper, nonlinear finite-element analysis (FEA) was handed to implement an in-depth examination on the behavior of concrete mid-rise walls reinforced with glass fiber reinforced polymer (GFRP) bars subjected to reversed cyclic loading while concurrently exposed to axial load. The FEA outcome was equated to the experimental outcomes of one GFRP-reinforced concrete mid-rise wall in-term of crack patterns, failure types and load–lateral displacement hysteretic response. A parametric research was then employed highlight the influence of longitudinal reinforcement ratio at wall boundary on diverse design features. It was displayed that the built model was steady and precisely simulated the experimentally stated behavior. The research also showed that while the boundary longitudinal reinforcement ratio had a remarkable effect on ultimate strength as well as the lateral stiffness, it slightly improved the energy dissipation capacity. Developing a technique with a noteworthy influence on energy dissipation that makes GFRP RC mid-rise walls competent to be used in strong seismic activity regions is indispensible.

 DOI: 10.21608/SEJ.2022.148445.1013

Keywords: Mid-rise shear wall, GFRP bars, FEM, cyclic load seismic.

1. INTRODUCTION

Reinforced-concrete (RC) walls with a height-to-length ratio (aspect ratio) ranging between 2.0 and 4.0 are frequently elaborated as the chief earthquake counterattacking element in mid-height constructions like parking garages as well as bridges. This form of walls is regularly nominated as mid-rise shear walls and their performance is dominant by flexural, even though the shear distortion has some impact on the whole behavior. Records from quakes registers have demonstrated that well-designed RC shear walls are effective and feasible as a major lateral-load-resisting system in response to wind as well as seismic activity loading [1]. In contrast to other lateral-resisting schemes, RC shear walls have established to provide outstanding and cost-efficient lateral resistance [1,2]. Freshly due to steel corrosion induced difficulties, fiber reinforced polymer (FRP) composites with non-corrodible characteristics have been advanced and used in dissimilar structures with an adequate behavior. Assumed their lower cost in comparison to other varieties of FRP bars, glass-FRP (GFRP) bars have established their way into various cast-in-place bridge surfaces [3-7].

Lately, with the increasing request for building constructions without corrosion concerns but with the forte, stiffness as well as deformation capacity essential to withstand earthquakes, an inclusive investigational campaign on the performance of concrete shear walls with FRP bars reinforcement has been piloted. The program started by Mohamed et al. [8] then concluded by Hassanein et al. [9] through constructing as well as testing shear walls with aspect ratio in the range of 2.0 → 4.0 and exclusively reinforced with GFRP bars. The chief variables were the aspect ratio of the walls as well as the confinement situation at the walls' boundary elements. It was stated that the tested walls demonstrated flexural failure instigated with concrete cover splitting shadowed with cover spalling and finished with concrete crushing at the wall toe under pressure. They moreover described that the properly designed shear walls with the new FRP bars can easily attain their ultimate strength whereas the objectionable failure modes (shear, sliding shear as well as anchorage failures) did not create a big dilemma and could be excellently dodged. Mohamed et al. [8] in addition to Hassanein et al. [9] added that the studied shear

* Corresponding author: attya85@yahoo.com

walls with GFRP reinforcement displayed high level of self-centering capability between load reversals up to the permissible drift limits indicated by diverse design codes. Nevertheless, some inquiries are still to be spoken for. For instance, the studied walls unveiled a very low efficiency in energy dissipation. As the longitudinal reinforcement ratio at the boundary components is a crucial consideration in mid-rise shear wall design, the offered paper is a statistical study that converses the impact of this parameter on the energy dissipation capability. Further wall performance indices like ultimate strength, drift capacity as well as failure mode are likewise discussed. A Finite element model repetitive for GFRP RC mid-rise walls was constructed and authenticated based on the obtainable experimental investigational outcomes. This is shadowed with a parametric study that encompassed the influence of longitudinal reinforcement ratio.

2. SUMMARY OF THE EXPERIMENTAL PROGRAM IN ADDITION TO THE OUTCOMES

To inspect the capability of the established FE model (FEM) in predicting the lateral response of mid-rise shear walls reinforced exclusively with GFRP longitudinal as well as transverse reinforcement, the foretold outcomes were matched to the experimental outcomes related to one well-detailed GFRP-reinforced mid-rise wall in the literature [9]. The wall was a full-scale mid-rise shear wall reinforced with GFRP bars and tested under the blend of lateral reversed cyclic and constant axial load. The studied GFRP-reinforced shear-wall sample was labeled as GnoX and created with 200 mm in depth, 1500 mm in length in addition to 3500 mm in height, occasioning in a model of a sole midrise shear wall. Table 1 states the used GFRP bars mechanical features. Table 2 states the reinforcement ratios as well as the measured concrete compressive strengths.

The scheme of reinforcement details in addition to the wall thickness meet the terms of CSA S806 [16], ACI 440.1R [17], CSA A23.3 [18] as well as ACI 318 [19]. The shear-wall samplings had two boundary components at both sides with dissimilar lengths as well as reinforcement ratios. Plane sectional examination was used to compute the flexural strength. Shear-wall samples were designed with an acceptable quantity of distributed as well as concentrated reinforcement to guarantee flexural domination also to inhibit shear as well as sliding-shear failures. Satisfactory shear reinforcement was delivered according to the CSA S806 [16] and the CSA A23.3 [18]. Detailed design calculations as well as processes can be found in Mohamed et al. [8]. The footing was profoundly reinforced with steel bars to evade any impact on the wall deformations throughout the assessments. The footing was used to fasten the sampling to a firm lab floor and assisted as an anchorage length for all vertical bars, because no lab splices were used. Additional details about the experiment setup as well as instrumentations can be found in [9].

TABLE 1. TENSILE PROPERTIES OF THE REINFORCEMENT [9]

Bar	Designated Bar Diameter (mm)	Nominal Area[1] (mm^2)	Tensile Modulus of Elasticity (GPa)	Tensile Strength[2]* (MPa)	Average Strain at Ultimate (%)
Straight bars					
#3 GFRP	9.5	71	62.5	1346	2.3
Bent #3 GFRP – rectilinear spiral					
Bent Portion	9.5	71	50	500	1.0
Bent #4 GFRP – horizontal bar					
Bent	12.7	126.7	50	500	---

[1]According to CSA S807 (CSA, 2010)
[2] Tensile properties were calculated using nominal cross-sectional areas.
*Guaranteed tensile strength: Average value – 3 × standard deviation (ACI 440.1R-15)
Note: 1 mm = 0.0394 in; 1 MPa = 145 psi

TABLE 2 – THE USED REINFORCEMENT RATIOS AND THE MEASURED CONCRETE STRENGTHS [9]

Wall	f_c' (MPa)	Reinforcement Ratio			
		ρ_l (%)	ρ_t (%)	ρ_v (%)	ρ_h (%)
GnoX	29.5	1.43	0.89	0.59	1.58

f_c' = concrete compressive strength; ρ_l = boundary longitudinal-bar reinforcement ratio; ρ_t = boundary-tie reinforcement ratio; ρ_v = web vertical-bar reinforcement ratio; ρ_h = horizontal web reinforcement ratio [9]

3. FINITE ELEMENT MODEL SIMULATION

Finite-element analysis (FEA) establishes an influential tool in modeling the behavior of experimentally structured elements and can harvest more comprehensive outcomes to be used in establishing a precise design model for such elements. Additionally, FEA can seize more detailed data that is challenging to monitor throughout investigational testing. A nonlinear 2D finite-element program, VecTor2, has been technologically advanced

among diverse formworks to realistically mimic the behavior of RC constructions, particularly those exposed to simulated seismic activity such as structural walls. The program engages a rotating-angle smeared-crack modeling methodology and uses the modified compression field theory (MCFT) [10]. VecTor2 foresees the behavior of steel reinforced shear walls, as well as GFRP-reinforced walls. Also more lately, hybrid reinforced walls (steel/GFRP bars) were validated in frequent research tests [11-15]. The practicability of VecTor2 to deliver trustworthy simulations, while engaging simple modeling practices, has been verified. The replicated models delivered precise calculations of wall-load capacities, pre- as well as post-peak displacement reactions, post-peak ductility, and chronology of damage as well as ultimate failure mode. In our research, VecTor2 was consequently adopted as an instrument to explore the influence of longitudinal reinforcement ratio at the wall boundary elements.

As displayed in Figure 1, Four-node quadrilateral elements were used to model the concrete. All reinforcement was exemplified smeared in concrete. Only, longitudinal reinforcement at the boundaries was replicated explicitly by truss elements. Succeeding the recommendation conveyed by Palermo and Vecchio [11], the height-to-length ratio of mesh elements was reserved less than 1.5 to dodge the localization effect. The convergence benchmarks were inspected based on iterative simulations of diverse meshes with diverse numbers of rudiments for the wall. Lateral displacement was put at the top of the rigid steel beam (height of 700 mm) that was separated into 7 mesh elements in the vertical course, while protecting the same horizontal discretization employed in the wall. The hysteric reaction of concrete was modeled based on Palermo and Vecchio [21]. The Hoshikuma et al. [22] parabola was employed in modeling the pre- as well as post-peak reaction of concrete, correspondingly. The concrete limitation delivered by the closed stirrups at the wall boundaries was deliberated based on Kupfer et al. [23]. The hysteretic characteristics of the steel reinforcement was exhibited agreeing with Seckin [24], while the stress–strain curve was established as linear for the GFRP reinforcement with a modulus equivalent to the elastic modulus of the GFRP reinforcement. The dowel action of steel bars was demonstrated employing He and Kwan [25]. The GFRP reinforcement's dowel action was disused according to ACI 440.1R [17]. The bond amid the reinforcing bars (GFRP) and concrete was demonstrated employing the modified Bertero–Eligehausen–Popov model [26]. These constitutive models of resources were embraced based on mathematical simulations for steel-reinforced squat walls [11] and GFRP-reinforced shear walls [27].

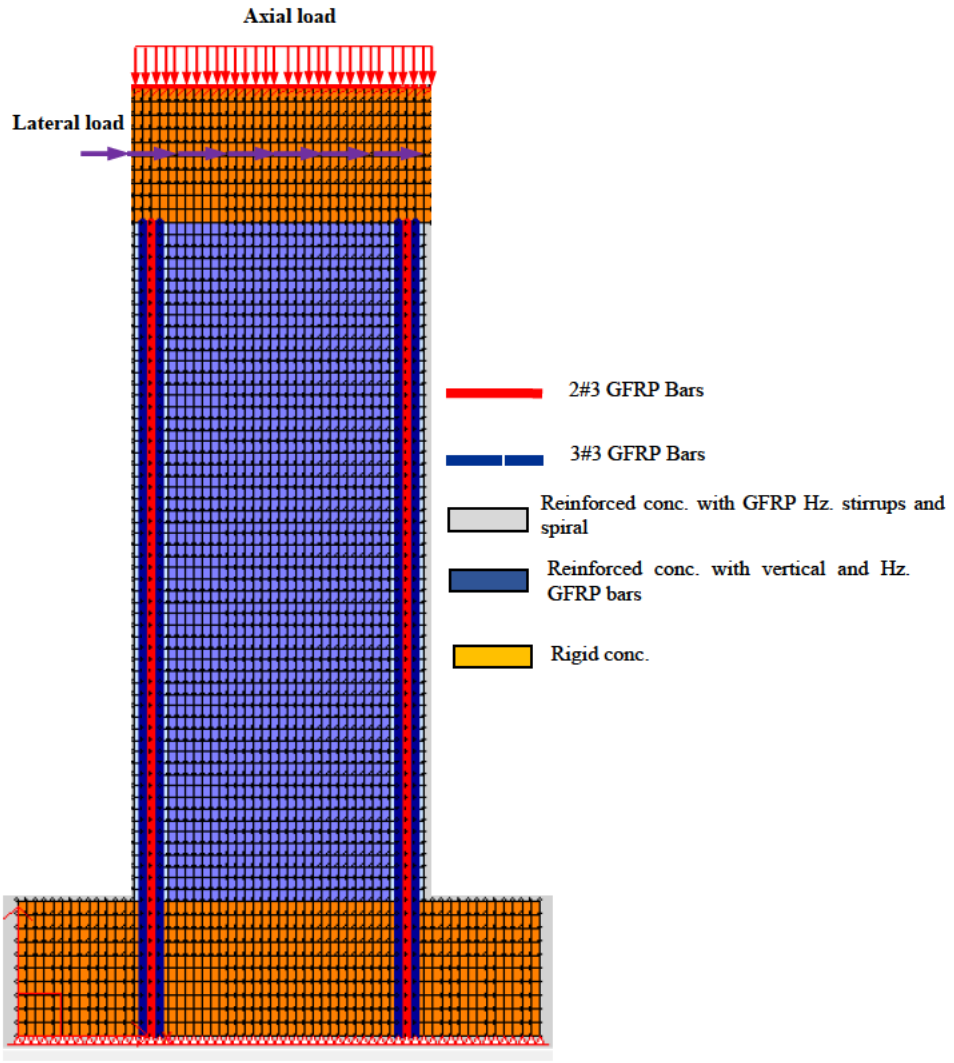

Fig. 1. Typical used mesh and truss elements for the modeled wall (GNoX)

3.1. Finite Element Model Calibration

Figures 2 matches the experimental as well as numerical outcomes in term of crack patterns and failure mode of the experimental sample. Like the experimentally conveyed outcomes, the simulated samplings revealed flexural cracks near the wall base. With further displacement, new flexural cracks formed at upper parts. Additional cracks grander height continued in appearance with more loading, whereas the former cracks amplified in length in addition to width. Under augmented displacement, the flexural cracks gained inclination down in the direction of the central zone of the web because of the effect of shear stresses. With extra increased loading, horizontal cracks complemented by inclined cracks sustained to spread, developing a fan shape as the crack inclination ranged in going close to the wall base. This deviation is attributable to the moment gradient alongside the wall height that affected the coordination of the prime stresses, which defines the shear-crack course. Employing further load, the concrete cover displayed splitting at the compression region then the cover spalled. Nonetheless, the wall persisted to carry loads without noticeable degradation as a consequence of the confinement at the wall boundaries. Eventually, the concrete crumpled and failure happened abruptly. Figure 2 validates the FEA precisely predicting the crack configuration in terms of intensity as well as inclination. Additionally, the program fruitfully foretells the cracks realign then close between load reversals that are accredited to the elastic characteristic of FRP bars. The conveyed simulation outcomes also reveal the capability of FEA in expecting the experimentally detected failure modes and concrete crushing at the walls border.

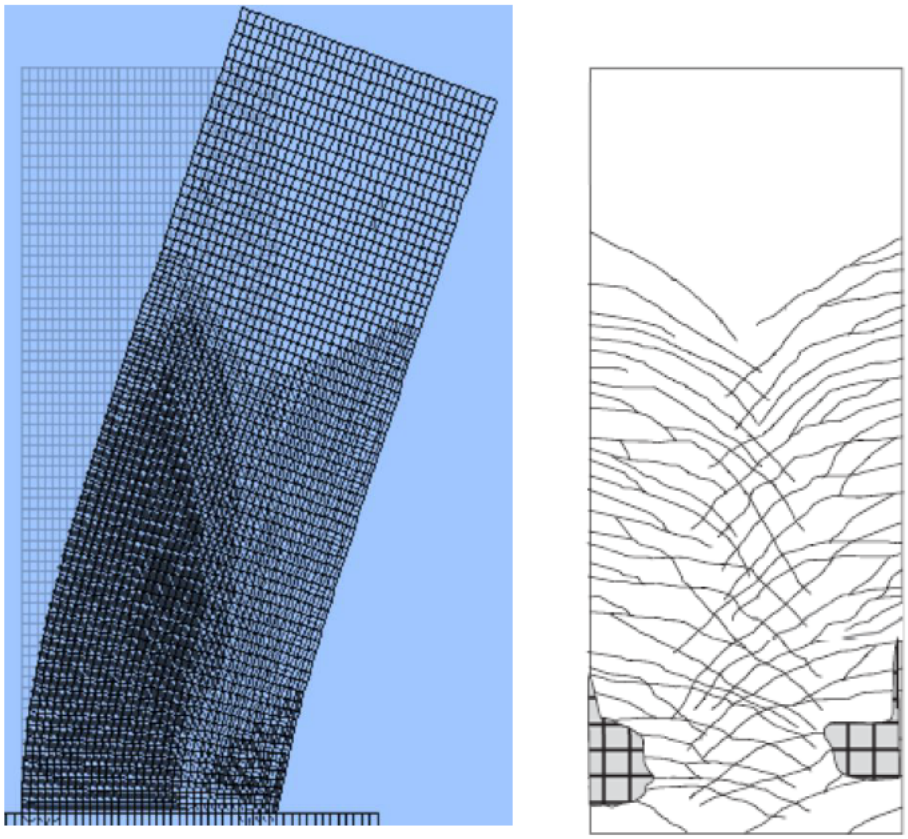

GnoX – FEA
Cracks pattern and failure mode

GnoX – experimental
Cracks pattern and failure mode

Fig. 2. Crack pattern, principal stress contours, and failure mode obtained from experimental and FEA results: wall GnoX

Figure 3 associates the experimental load-drift ratio hysteretic response to FEA ones. The primary stiffness of the simulated wall was nearly identical to the investigational outcomes up to the first flexural cracks dissemination. Both the FEM model as well as experimental citations had comparable load corresponding to the first flexural cracks commencement. As exhibited in Table 3, the variance between the first experimental and numerical flexural-cracking load was 5%. This is imperative chiefly for the cracked-lateral stiffness scheming. The sampling demonstrated a noteworthy reduction of stiffness subsequent to the first flexural cracks that was precisely seized in the numerical model. As exhibited in Figure 3, both the experimental as well as numerical models displayed a progressive minor dilapidation in the lateral stiffness owing to the development of additional flexural and/or shear-flexural cracks with analogous tendencies to failure. It is of importance to assess the competence of the model to seize the hysteretic loop of GFRP RC wall. By performing so, the scholars went through the literature and realized the subsequent points that branded the hysteric reaction of GFRP walls [8, 19]:

1. The hysteric loops are tight
2. The unloading/reloading curves revealed linearity liable on GFRP elastic conduct.
3. The reloading branches trailed a similar loading course but at a lesser loading stiffness, causing lower peak power.
4. The unloading path form seems to be reliant on the strain at the onset of unloading.
5. The loops progressively widen with concrete cover splitting as well as spalling with residual deformation instigated by concrete degradation in cyclic loading.

Figure 4 demonstrates a close-up of the FEA hysteric loops model. Undoubtedly, the portrayed hysteric loops back up the literature documentations. Table 3 portrays the experimentally as well as analytically foretold ultimate loads, drift ratios. The ratios amongst the experimentally achieved ultimate loads as well as drift ratios to their numerically computed values reveal that the rational simulation as the regular difference amidst the predicted as well as experimental outcomes was within 10%.

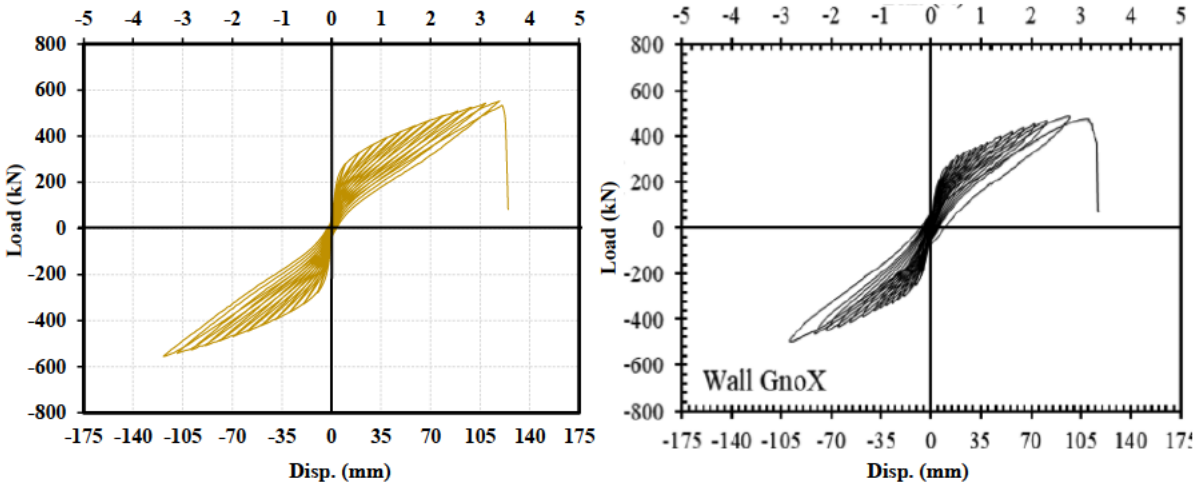

a) GnoX – FEA
Load-drift ratio hysteretic response

b) GnoX – Exp.
Load-drift ratio hysteretic response

Fig. 3. load-drift ratio hysteretic response for Experimental versus FEA: wall GnoX

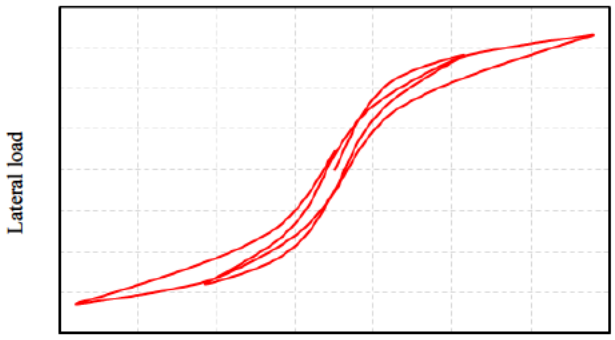

Fig. 4. Typical load-displacement hysteric cycle for GFRP RC walls (Numerical model)

TABLE 3 – FE MODEL VALIDATION RESULTS

Wall ID	Experimental			FEA.			$\frac{P_{fpred}}{P_{f\,exp}}$	$\frac{P_{upred}}{P_{u\,exp}}$	$\frac{d_{upred}}{d_{u\,exp}}$
	P_{fexp} (kN)	P_{uexp} (kN)	d_{uexp} (%)	P_{fpred} (kN)	P_{upred} (kN)	d_{upred} (%)			
GnoX	196	498	3.32	206	540	3.56	1.05	1.08	1.07

Notes: P_{fexp} = the experimental first flexural cracking load, P_{uexp} = the experimental ultimate load, d_{uexp} = the experimental drift ratio corresponding to ultimate load, $E_{uexp.}$ = the experimental cumulative energy dissipation at failure, $P_{fpred.}$ = the predicted first flexural cracking load, P_{upred} = the predicted ultimate load, d_{upred} = the predicted drift ratio corresponding to ultimate load, $E_{upred.}$ = the predicted cumulative energy dissipation at failure.

Figure 5 associates the load-drift ratio envelop curves acquired from investigational versus numerical outcomes. The numerical outcomes exhibited just about the same lateral stiffness described experimentally with

a lateral drift ratio up to 3%. Incidentally, this ratio was abundantly greater than the supreme permissible listed drift ratio for shear walls in diverse design codes as well as guiding principle (2.5%). Conclusively, the model calibration maintains that the prototype can precisely simulate the cyclic reaction of mid-rise walls.

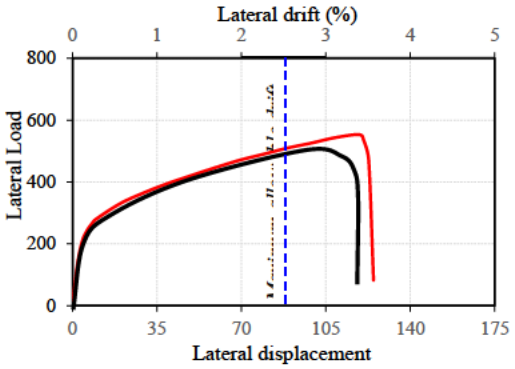

Fig. 5. Load-drift ratio envelop curves for Experimental versus FEA: wall GnoX

4. ANALYSIS BASED ON FEA

4.1. Boundary Longitudinal Reinforcement Ratio Result

Design provisions for longitudinal reinforcement arrangements of mid-rise RC walls are founded on the plane section theory. Such a theory commonly postulates wall layouts with boundary elements comprehending large volumes of vertical reinforcement, employing advanced moment resistance as well as a greater deformation capability than the same reinforcement disseminated consistently alongside the wall length. Henceforth it is of importance to assess the impact of such aspect on the wall performance bearing in mind the failure mode, ultimate strength, drift capacity, stiffness, residual displacement as well as the energy dissipation capacity. Attending to this objective, two longitudinal reinforcement ratios were studied: 2.53% as well as 3.95%, along with the vertical web reinforcement ratio of 1.43% employed in GnoX. This was accomplished by substituting the vertical #3 GFRP bars with #4 in addition to #5 bars, in turn, whereas maintaining the unchanged horizontal web reinforcement ratio with the similar mechanical features. It should be distinguished that the reinforcement ratio was premeditated bearing in mind the boundary dimensions as 200mm × 200mm. For easiness of reference, the samplings were labeled as G3, G4, and G5, in that order.

4.1.1. Effect on Crack Patterns as well as Failure Mode

Figure 6 matches the crack patterns in addition to failure mode of the exhibited samples. The FEA outcomes mostly validated that growing the boundary longitudinal reinforcement ratio had no consequence on the failure mode, as the three samplings went under flexural compression failure. Breakage of the concrete at compression region trailed with cover spalling shadowed by concrete crushing after numerous cycles is owed to the transverse reinforcement influence. The key variance amid the three samples was the altitude at which the cracks disseminated; the greater the longitudinal reinforcement ratio, the greater elevation at which the cracks spread. This is accredited to the increased load capacity accomplished in the samples with greater longitudinal reinforcement ratio. Furthermore, the outcomes evidently displayed that height at which concrete collapsed is higher as the longitudinal reinforcement amplifies. This was as well owed to the greater load capacity.

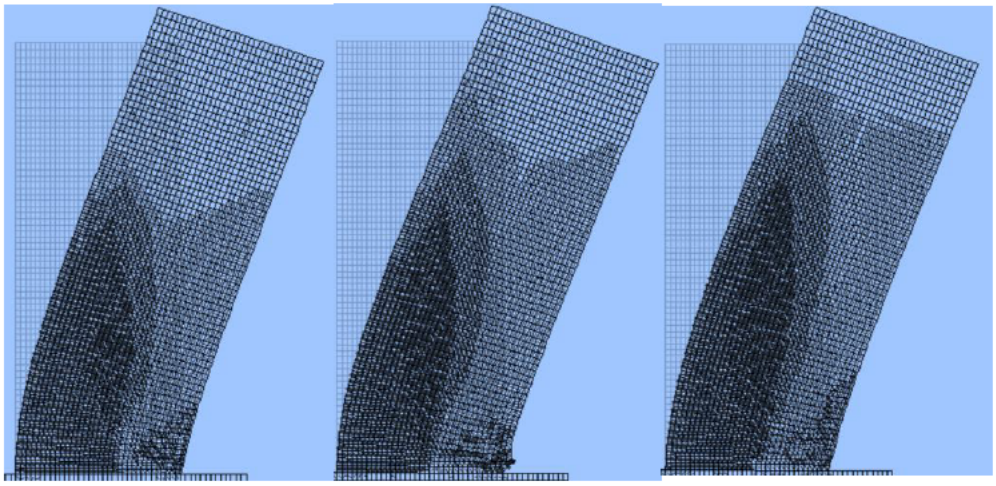

Fig. 6. Cracks pattern and failure of specimens G3, G4, and G5.

4.1.2. Effect on Load-drift Ratio Hysteretic Response

Figure 7 demonstrates the load-drift ratio hysteric reaction for the three exhibited samplings. No noteworthy alteration in the loop cycles can be detected. The marginal variation is that the greater the reinforcement ratio, the more constricted the hysteric loops become. This is accredited to the larger quantity of GFRP with elastic characteristics that ruled the behavior and made a minimal residual deformation. The hysteric loops profile did not vary from the designated form (Fig. 4) except for increased pinched behavior recognized.

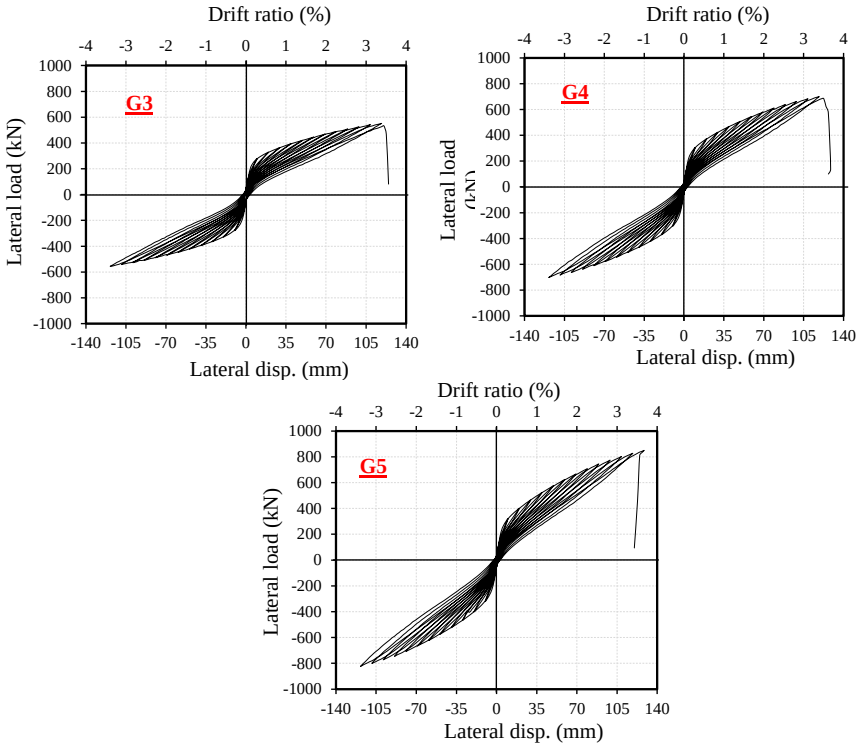

Fig. 7. Load-displacement hysteretic response for the simulated specimens

4.1.3. Effect on Lateral Stiffness and Ultimate Strength

Figure 8 parallels the lateral load–drift ratio envelope curves for the three exhibited samples. The reinforcement ratio did not demonstrate any impact on the preliminary flexural stiffness up until the load at which the first flexural fissures disseminated. A very minor variance within 2-3% accredited to the greater moment of inertia was perceived as a result of the greater longitudinal reinforcement ratio. For the fissured case, the reaction seems to be altered since noticeable higher lateral stiffness in samplings with greater longitudinal reinforcement ratio was apparent. This can be a benefit since the displacement demand can be condensed. The influence was as well prominent on the ultimate strength (57% strength increase in sample G5 compared to G3), whilst the influence on drift capacity was insignificant.

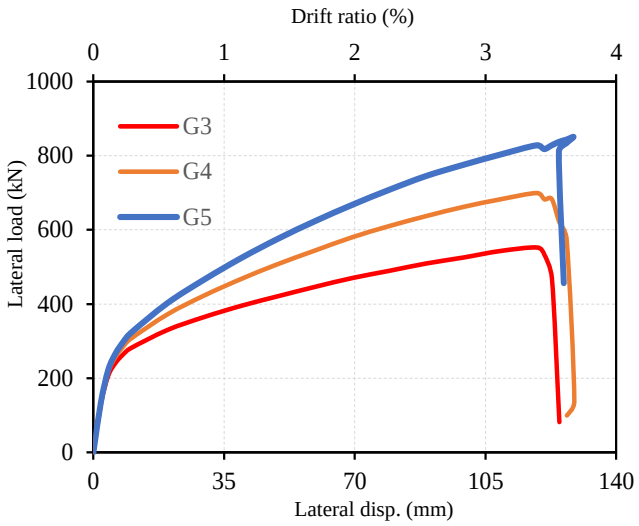

Fig. 8. The envelop curves of load-displacement hysteretic response for the simulated specimens

4.1.4. Effect on Energy Dissipation

Energy dissipation is an imperative guide for construction design in seismic activity areas as it lessens the earthquake force on buildings. This index institutes a big dilemma in designing GFRP assemblies in strong seismic activity areas that may obstruct their employment in such regions. For that reason, it is of concern to assess the influence of longitudinal reinforcement ratio as a changeable on the energy dissipation capability. For this drive, the collective energy dissipation was premeditated for each sample by adding the dissipated energy values in successive load–displacement loops till failure in addition to plotting counter to drift ratio (**Fig. 9**). Analogous accumulative energy dissipation was attained by the three samples nonetheless the longitudinal reinforcement ratio, even though the sampling with high reinforcement ratio demonstrated minor development but the outcome is still minimal.

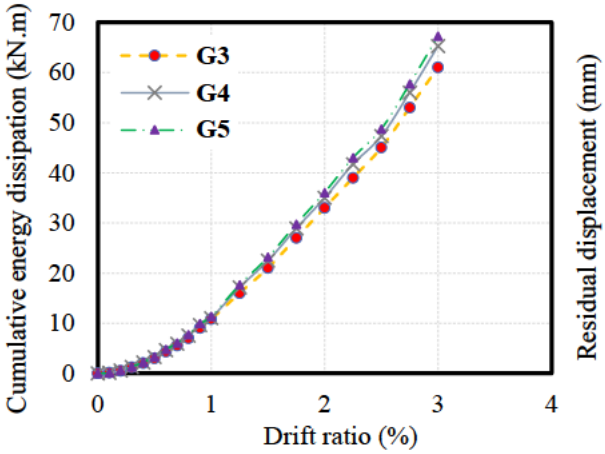

Fig. 9. Drift ratio versus cumulative energy dissipation

5. DISCUSSION AND DEDUCTIONS

This research exemplifies a step onward employing the finite-element method (FEM) as a potent tool to simulate the performance of GFRP RC mid-rise walls under earthquakes that have been experimented and validated their viability in low-to-moderate seismic activity regions. A numerical finite-element model was instigated and calibrated compared to the experimental study outcomes of one experimented GFRP RC mid-rise wall accessible in the literature. The study was corroborated and displayed the competency of the model in seizing the focal behavioral aspects. The research was then prolonged to examine the influence of the boundary longitudinal reinforcement ratio. The subsequent concluding annotations could be drawn:

1. Elevated longitudinal FRP reinforcement ratio at the wall boundary considerably enriched the lateral stiffness in addition to the ultimate strength, whilst it had a minimal influence on energy dissipation.
2. An alternate operational approach for energy dissipation development is compulsory in GFRP RC mid-rise walls to increase its practicability in strong seismic activity zones.

References

[1] Fintel, M. (1995). "Performance of Buildings with Shear Walls in Earthquakes of the Last Thirty Years," PCI Journal, 40 (3), 62-80.

[2] Cardenas, A. E. Hanson, J. M.; Corley, W. G.; and Hognestad, E. (1973). "Design Provisions for Shear Walls," *ACI Journal Proceedings*, 70(3), 221-230.

[3] Bradberry, T. E. (2001). "Concrete Bridge Decks Reinforced with Fiber Reinforced Polymer Bars." *Transportation Research Record*, 1770, 94–104.

[4] Nanni, A., and Faza, S. (2002). "Designing and Constructing with FRP Bars: an Emerging technology." ACI Concrete Institutions., 24(11), 53–58.

[5] El-Salakawy, E., Benmokrane, B., El-Ragaby, A., and Nadeau, D. (2005). Field investigation on the first bridge deck slab reinforced with glass FRP bars constructed in Canada." Journal of Composit for Construction., 6(470), 470–479.

[6] Benmokrane, B., El-Salakawy, E., El-Gamal, S., and Goulet, S. (2007). "Construction and testing of an innovative concrete bridge deck totally reinforced with glass FRP bars: Val-Alain Bridge on Highway 20 East." Journal of Bridge Engineering, 5(632), 632–645.

[7] Arafa, A., Farghaly, A., Ahmed, E., and Benmokrane, B. (2016). "Laboratory Testing of GFRP-RC Panels with UHPFRC Joints of the Nipigon River Cable-Stayed Bridge in Northwest Ontario, Canada." *Journal of Bridge Engineering*, 10.1061/(ASCE)BE.1943-5592.0000943, 05016006.

[8] Mohamed, N., Farghaly, A. S., Benmokrane, B. and Neale, K. W. (2014). "Experimental Investigation of Concrete Shear Walls Reinforced with Glass-Fiber-Reinforced Bars underLateral Cyclic Loading." *Journal of Composites for Constructions*, 18 (3): 04014001.

[9] Hassanein A., Mohamed N., Farghaly A. S., and Benmokrane B. (2019). "Experimental Investigation: New Ductility-Based Force Modification Factor Recommended for Concrete Shear Walls Reinforced with Glass Fiber-Reinforced Polymer Bars." *ACI Structural Journal*, 116(1), 213-224.

[10] Vecchio, F. J., Collins, M. P. (1986). "Modified Compression Field Theory for Reinforced Concrete Elements Subjected to Shear." *ACI Structural Journal*, 83(2), 219-231.

[11] Palermo, D., and F. J. Vecchio. (2007). "Simulation of cyclically loaded concrete structures based on the finite-element method." Journal of Structural Engieering, 133 (5): 728–738.

[12] Gulec, C. K., and Whittaker, A., S. (2009). Performance-based assessment and design of squat reinforced concrete shear walls. New York: Multidisciplinary Center for Earthquake Engineering Research.

[13] Vecchio, F. J., and I. McQuade. (2011). "Towards improved modeling of steel-concrete composite wall elements." Nucl. Engineering Design Journal, 241 (8), 2629–2642.

[14] Mohamed, N., A. S. Farghaly, B. Benmokrane, and K. W. Neale. (2014). "Numerical Simulation of Mid-Rise Concrete Shear Walls Reinforced with GFRP Bars Subjected to Lateral Displacement Reversals." Engineering Structures, 62–(71).

[15] Ghazizadeh, S., C. A. Cruz-Noguez, and F. Talaei. (2018). "Analytical Model for Hybrid FRP-Steel Reinforced Shear Walls." Engineering Structures Journal,. https://doi.org/10.1016/j.engstruct.2017.11.060.

[16] Canadian Standards Association (CAN/CSA). (2012). "Design and Construction of Building Components with Fiber-Reinforced Polymers." S806, CSA, Mississauga, ON, Canada, 208pp.

[17] ACI Committee 440. (2015). "Guide for the Design and Construction of Structural Concrete Reinforced with Fiber-Reinforced Polymer (FRP) Bars." ACI 440.1R-15, Farmington Hills, MI.

[18] Canadian Standards Association (CAN/CSA). (2014). "Design of concrete structures standard." A23.3, CSA, Mississauga, ON, Canada, 240.

[19] ACI Committee 318. (2014) "Building Code Requirements for Structural Concrete and Commentary (ACI 318-14)," American Concrete Institute, Farmington Hills, MI, 503 pp.

[20] Wong, P. S., and F. J. Vecchio. (2002). VecTor 2 and formworks user's manuals, 213. Toronto: Dept. of Civil Engineering, Univ. of Toronto.

[21] Palermo, D., and F. J. Vecchio. 2002. "Behavior of Three-Dimensional Reinforced Concrete Shear Walls." *ACI Struct. J.* 99 (1): 81–89.

[22] Hoshikuma J, Kawashima K, Nagaya K, Taylor AW. Stress-strain model for confined reinforced concrete in bridge piers. J Struct Eng, ASCE 1997;123(5):624–33.

[23] Kupfer H, Hilsdorf HK, Rusch H. Behavior of concrete under biaxial stress. ACI J 1969;87(2):656–66.

[24] Seckin M. Hysteretic behaviour of cast-in-place exterior beam-column-slab subassemblies. Ph.D. Thesis, Department of Civil Engineering, University of Toronto, Toronto, ON, Canada; 1981. p. 266.

[25] He, X. G., and A. K. H. Kwan. 2001. "Modeling dowel action of reinforcement bars for finite element analysis of concrete structures." Comput. Struct. 79 (6): 595–604.

[26] Eligehausen, R., E. Popov, and V. Bertero. 1983. Local bond stress-slip relationship of deformed bars under generalized excitations. Rep. No. UCB/EERC-83/23. Berkeley: Earthquake Engineering Center, Univ. of California.

[27] Arafa, A., A. S. Farghaly, and B. Benmokrane. 2018b. "Nonlinear Finite-Element Analysis for Predicting the Behavior of Concrete Squat Walls Reinforced with GFRP Bars." J. Struct. Eng. 22 (2).